Supporting Information

Data collection and processing	**Tar-turnover-1**	**Tar-turnover-2**
Energy filters & detector	BioQuantum / K3	BioQuantum / K3
Energy window (eV)	20	20
Magnification (nominal)	130,000 x	130,000 x
Voltage (kV)	300	300
Electron exposure per movie ($e^-/Å^2$)	50	50
Exposure Time (s)	1.49	1.49
Exposure rate (e/pix/s)	15	15
Electron exposure per frame ($e^-/Å^2$/frame)	1.25	1.25
Defocus range (μm)	-0.6 : -2.2	-0.6 : -2.2
Pixel size (Å)	0.66	0.66
Symmetry	C1	C1
Initial particle images (No.)	2,939,835	2,939,835
Final particle images (No.)	211,906	122,001
Map resolution (Å)	3.1	3.2
FSC threshold	0.143	0.143
Map resolution range (Å)	2.3-36.0	2.2-37.4
Model refinement		
Model resolution (Å)	3.3	3.4
FSC threshold	0.5	0.5
Map sharpening B factor ($Å^2$)	-114.9	-117
Model composition		
Non-hydrogen atoms	9,016	9,198
protein residues	1,138	1,142
Ligands	Tar:1; ATP:2; CLR:2	Tar:1; Mg^{2+}:2; PC:2: ATP:2; CLR:4
B factors ($Å^2$)		
protein	29.2/81.4/48.2	43.9/93.0/60.9
ligand	28.7/61.8/43.5	47.2/71.7/56.8
RMSD		
Bond lengths (Å)	0.007	0.005
bond angles (°)	0.632	0.599
Validation		
MolProbity score	1.28	1.29
Clash score	3.97	2.63
Poor rotamers (%)	0.41	0.2
Ramachandran plot		
Favored (%)	97.5	96.35
Allowed (%)	2.32	3.48
Disallowed (%)	0.18	0.18
PDB	8BHT	8BI0
EMDB	EMD-16069	EMD-16075
Job	J16	J15

Table S1: Cryo-EM data collection, refinement and validation statistics

Systems	Ligand	State	# replicas	time per replica	Total time
1	topotecan	TO1	2	2 μs	4 μs
2	topotecan	TO2	2	2 μs	4 μs
3	tariquidar	TO1	2	2 μs	4 μs
4	tariquidar	TO2	2	2 μs	4 μs
5	-	Apo	2	1 μs	2 μs

Table S2: **Simulated systems.** Structures in TO1 and TO2 states were simulated in the presence of different ligands, topotecan or tariquidar, or in the apo form. Each system was replicated with different initial lipid placements, and simulated for 2 μs for turnover states and 1 μs for apo state.

Systems	Bound ligand	State	Volume (Å^3)
1	topotecan	TO1	3,298
2	topotecan	TO2	979
3	tariquidar	TO1	2,742
4	tariquidar	TO2	669

Table S3: **Binding pocket unoccupied volume.** Unoccupied space of the binding pocket calculated in the presence of topotecan or tariquidar for the TO1 and TO2 states, using POVME 2.0 [91] with 0.5 Å grid spacing.

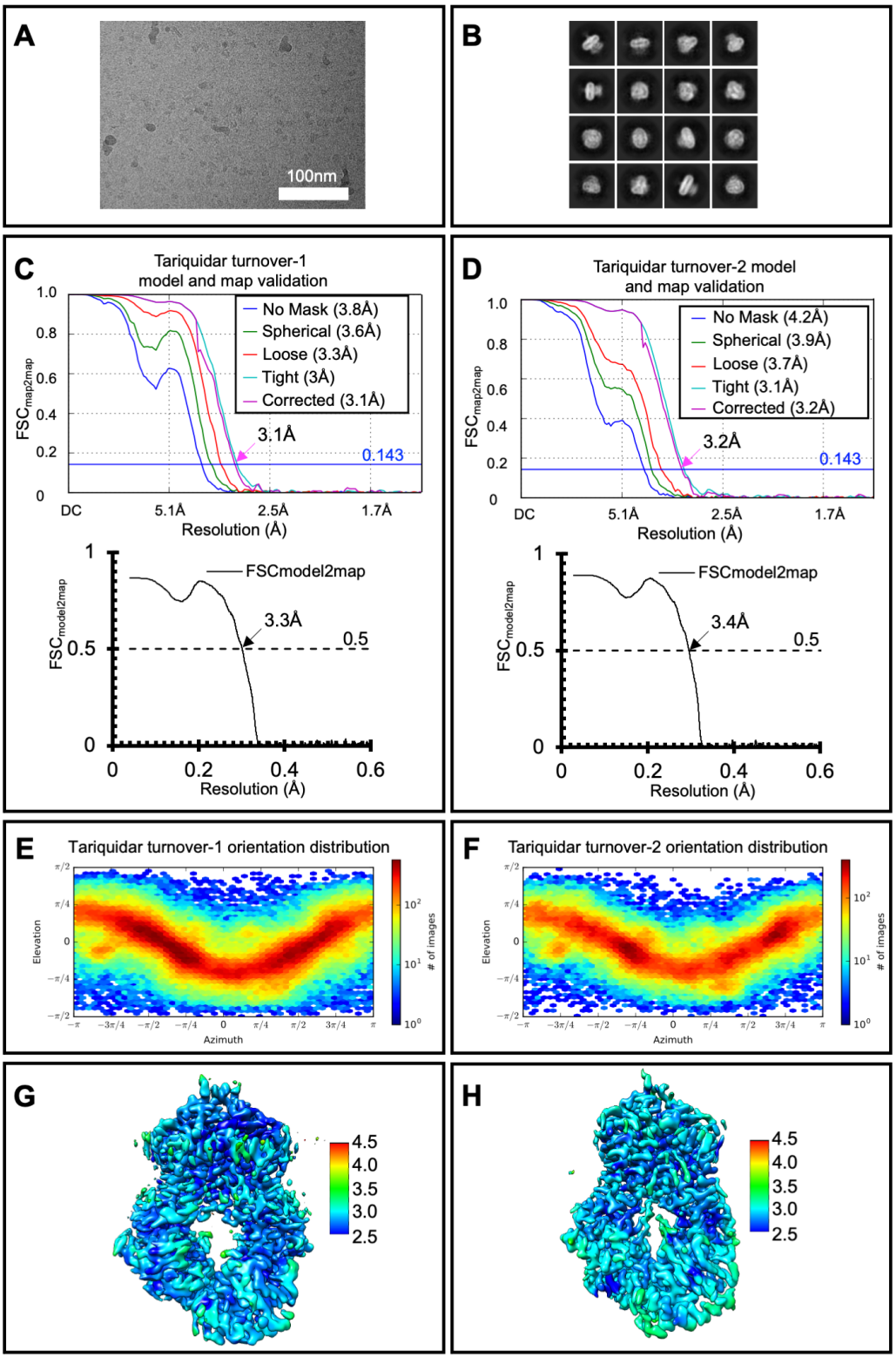

Figure S1: continued on the next page

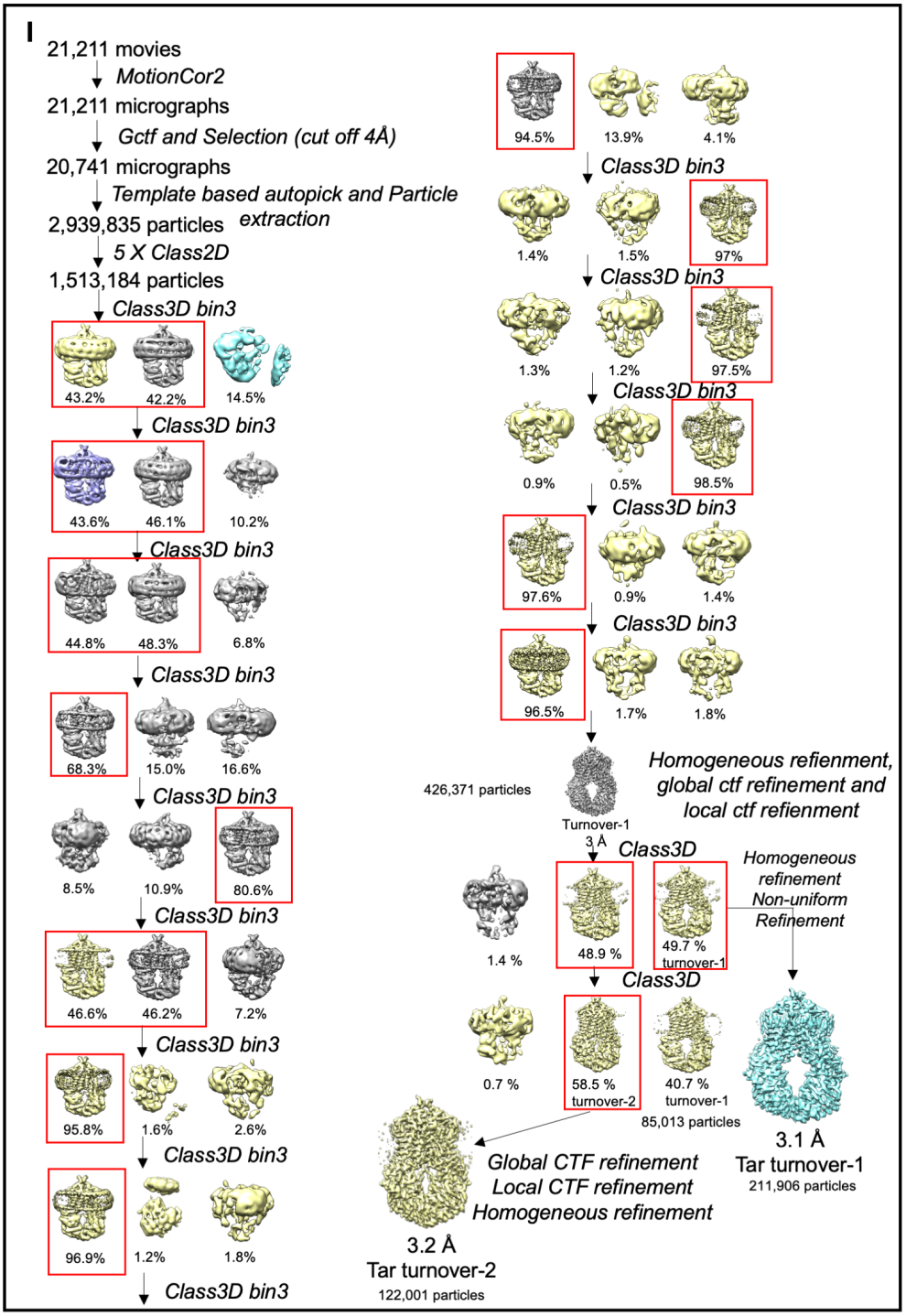

Figure S1: **Cryo-EM data processing for ABCG2 tariquidar turnover samples**. **(A)** Representative motion-corrected 2D micrograph of a tariquidar turnover sample image among 21,211 images collected. White scale bar, 1000 Å. **(B)** Representative 2D classes. **(C)** Map and model validation of the tariquidar TO1 structure. **(D)** Map and model validation of the tariquidar TO2 structure. **(E, F)** Angular distribution plots of tariquidar turnover-1 and turnover-2 structures. **(G, H)** Local resolution of tariquidar TO1 and TO2 structures. FSC: Fourier shell correlation. **(I)** Flowchart of data processing of the tariquidar turnover samples. Red boxes indicate classes of particles selected for the next round.

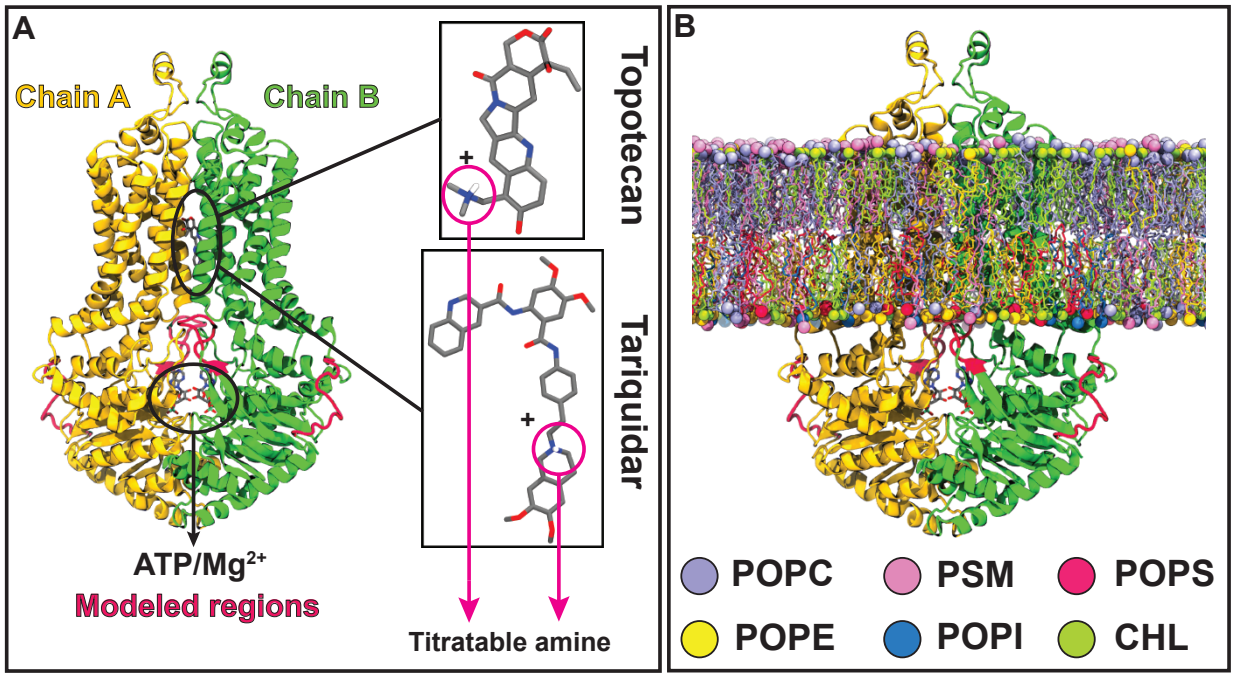

Figure S2: **Initial system setup for MD simulations. (A)** ATP/Mg^{2+}-bound ABCG2 structure prepared for MD simulations. Chains A and B are colored orange and green, respectively. The two missing disordered regions which were modeled and added to the system are shown in red. ATP/Mg^{2+} and substrate binding sites are highlighted with black ovals. The simulations were conducted for ligand-bound TO1 and TO2 states, as well as the IF-apo conformation. In ligand-bound simulations, each ligand contains a titratable amino group (magenta circles), which is protonated under physiological pH, resulting in a net +1 charge for each ligand. **(B)** Membrane-embedded protein system. A mixed lipid bilayer composed of POPC, POPE, POPS, POPI, POPA, PSM, and cholesterol (CHL), at molar ratios of 39:6:0:0:0:21:34 and 17:25:11:8:1:9:29 in the extracellular and cytoplasmic leaflets, respectively, was used in all simulations.

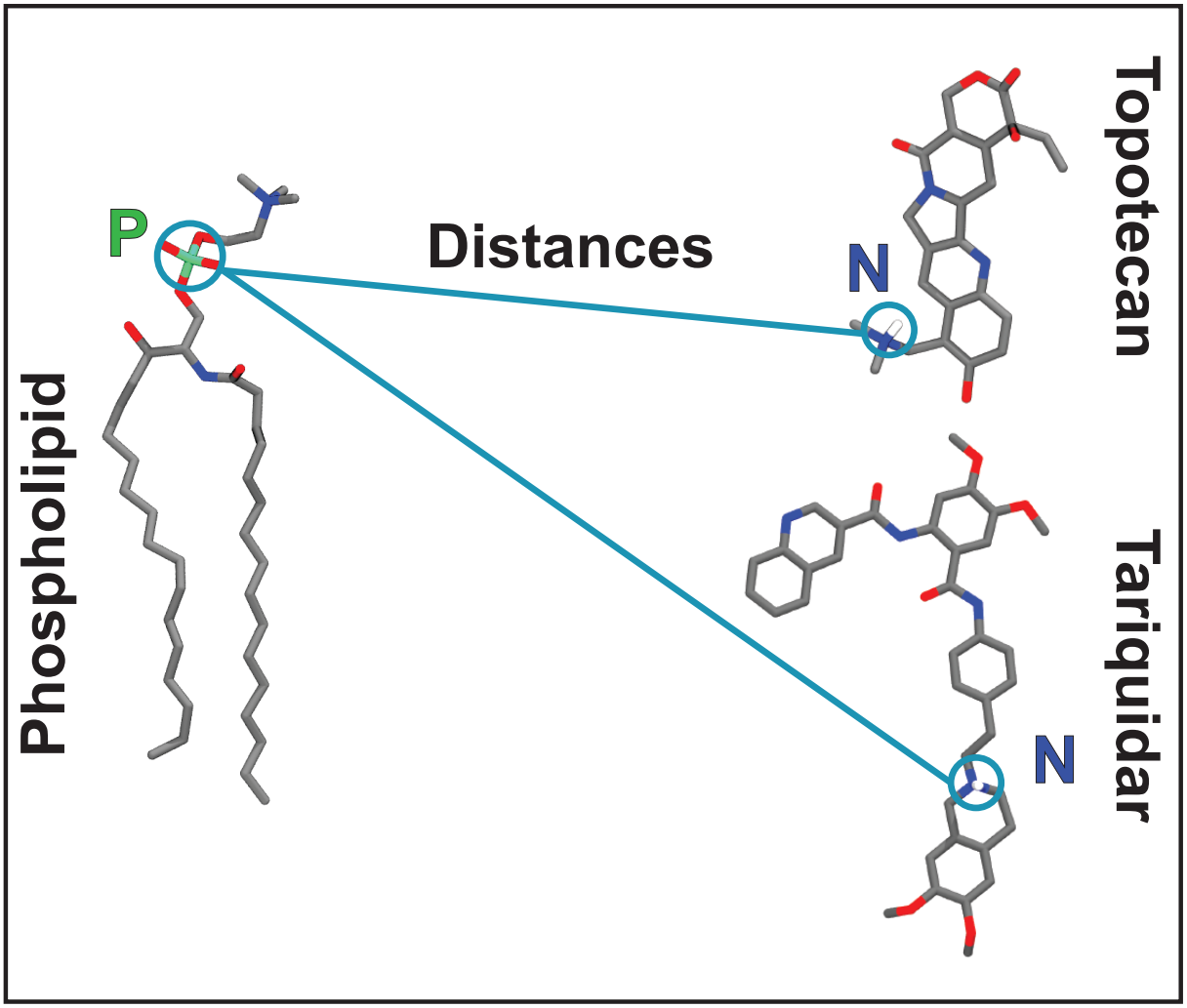

Figure S3: **The specific distance used for identifying lipids in the ligand binding pocket**. Chemical structures of a representative phospholipid and the the two substrates, topotecan and tariquidar. proximity of a lipid was determined using the distance between the phosphorus atom of the phospholipid (P) and the nitrogen atom of the titratable amine (N) in each ligand.

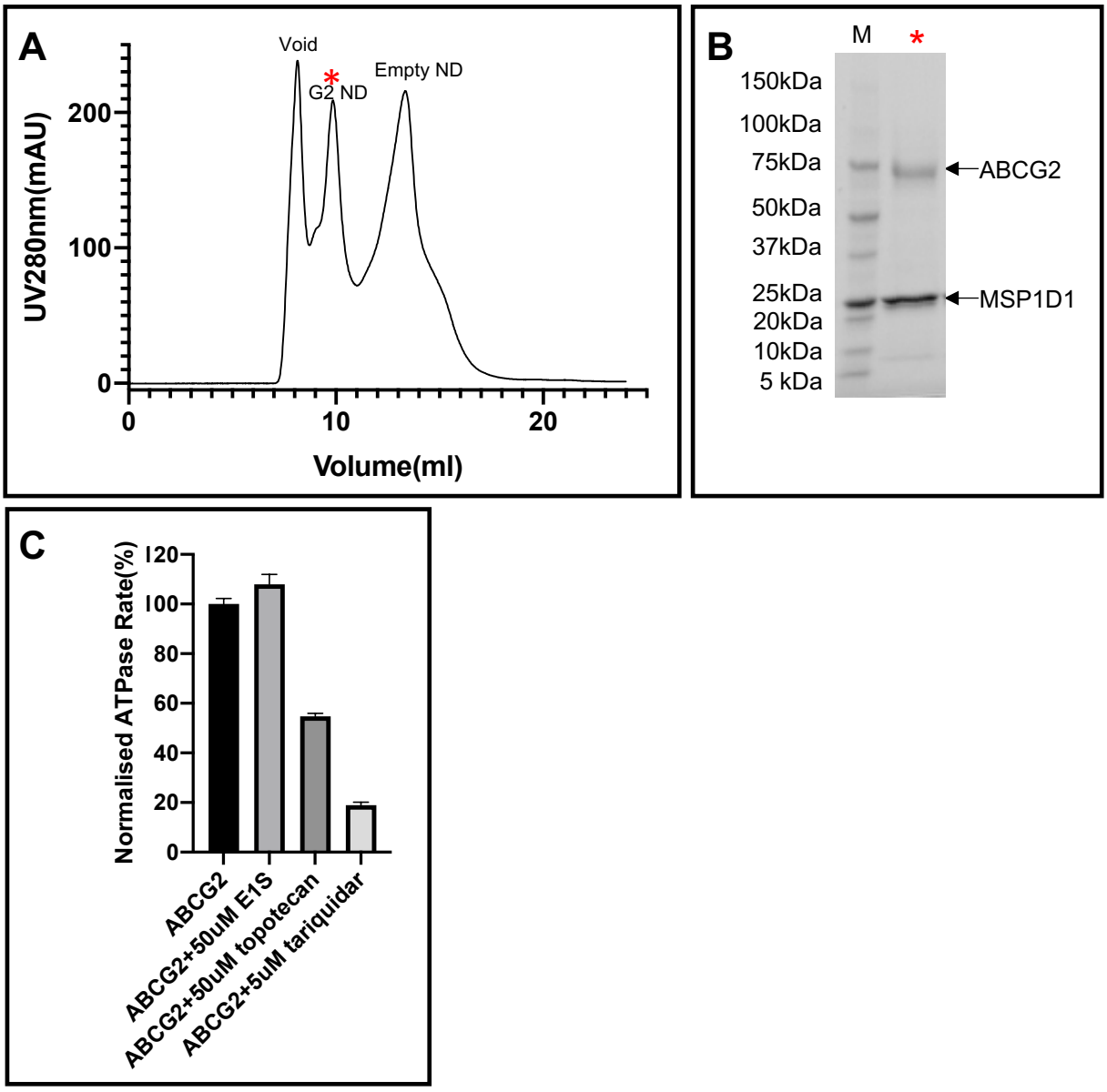

Figure S4: **Nanodisc-reconstituted ABCG2 and its ATPase activity**. **(A)** A representative gel filtration profile of nanodisc-reconstituted ABCG2. Void indicates void peak; empty ND indicates the peak for empty nanodisc and red Asterisk indicates the ABCG2 nanodisc peak. **(B)** A representative SDS-PAGE analysis of main peak obtained in gel filtration. Reducing agent was used, and ABCG2 ran as a monomer. M shows marker proteins, with masses indicated on the left. The red asterisk shows the peak fraction analyzed in the gel and used for EM grid preparation. **(C)** ATPase activity of nanodisc-reconstituted wild-type ABCG2 in the presence and absence of 50 μM E_1S, 50 μM topotecan, or 5 μM tariquidar. ATPase rate is normalized with respect to the activity of apo ABCG2 nanodiscs (the ATPase rate of apo ABCG2 nanodisc is set to 100%). The bars show mean rates. The experiment in each case was performed 3 times independently with the sample batch of nanodiscs ($n = 3$); error bars depict standard deviations (s.d.).

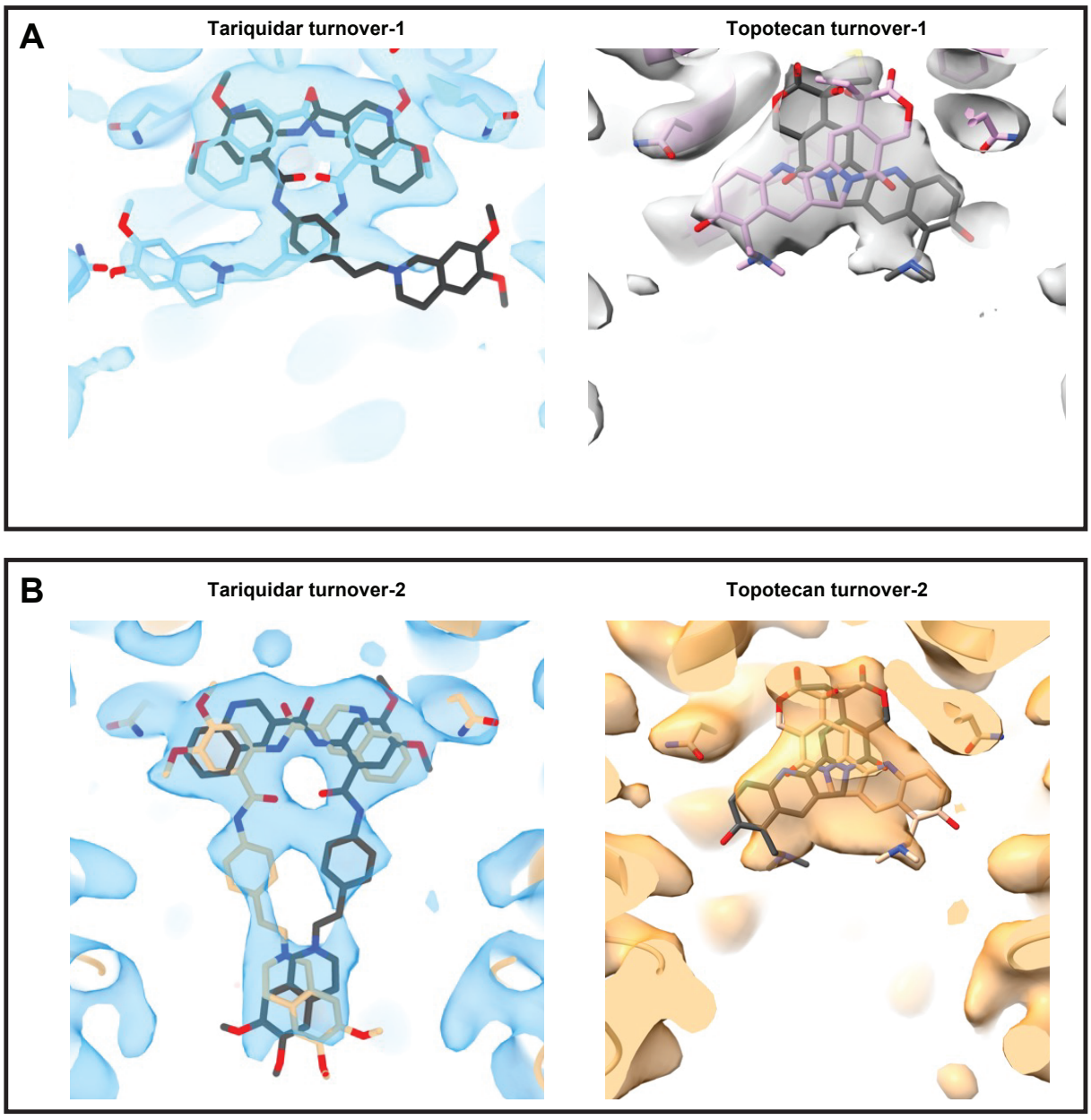

Figure S5: **Comparison of cryo-EM densities of substrates and alternative binding poses of substrates in ABCG2 turnover structures**. **(A)** Tariquidar (left) and topotecan (right) in TO1 state. **(B)** Tariquidar (left) and topotecan (right) in TO2 state. EM densities are shown as transparent surfaces, and substrates are shown as sticks. The symmetry-related, alternative binding pose of substrates are shown as black sticks.

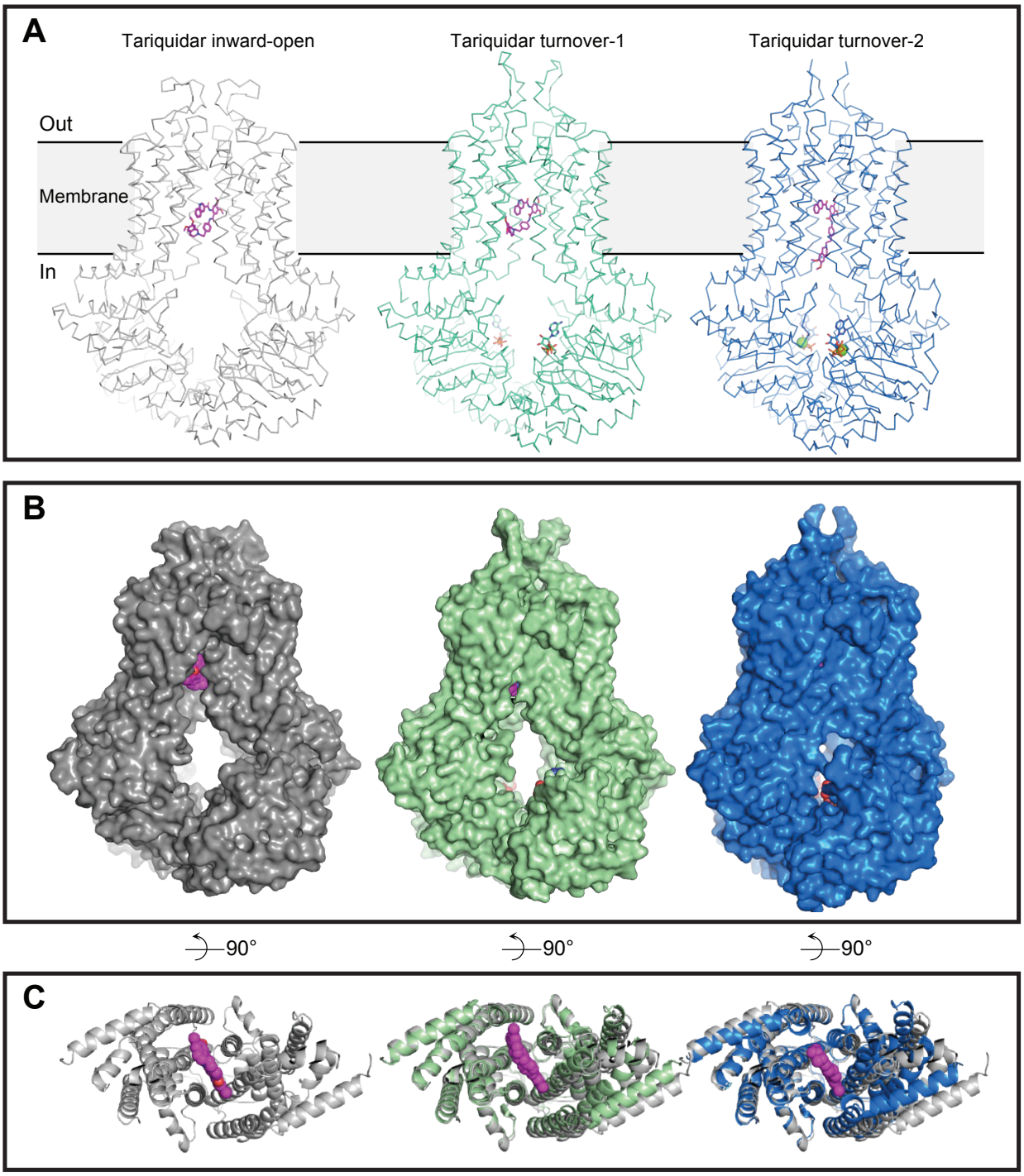

Figure S6: **Structural comparison between tariquidar-bound TO1 (green), TO2 (blue), and IF-open (gray) conformations of ABCG2**. **(A)** Overview of tariquidar-bound ABCG2 structures in ribbon presentations. Left, inward-open conformation; middle, tariquidar TO1 state; right, tariquidar TO2 state. Bound ligands are shown in sticks. **(B)** Tariquidar bound ABCG2 structures in surface presentations. Bound tariquidar are shown in magenta spheres. The order for the structures are the same as in **A**. **C** Cytoplasmic view of ABCG2-TMD. The left TMD in TO1 or TO2 structures are superimposed on the equivalent TMD in tariquidar inward-open structure. This emphasizes the conformational differences between tariquidar-bound turnover states of TO1, TO2 and the tariquidar-bound inward-open conformation of ABCG2.

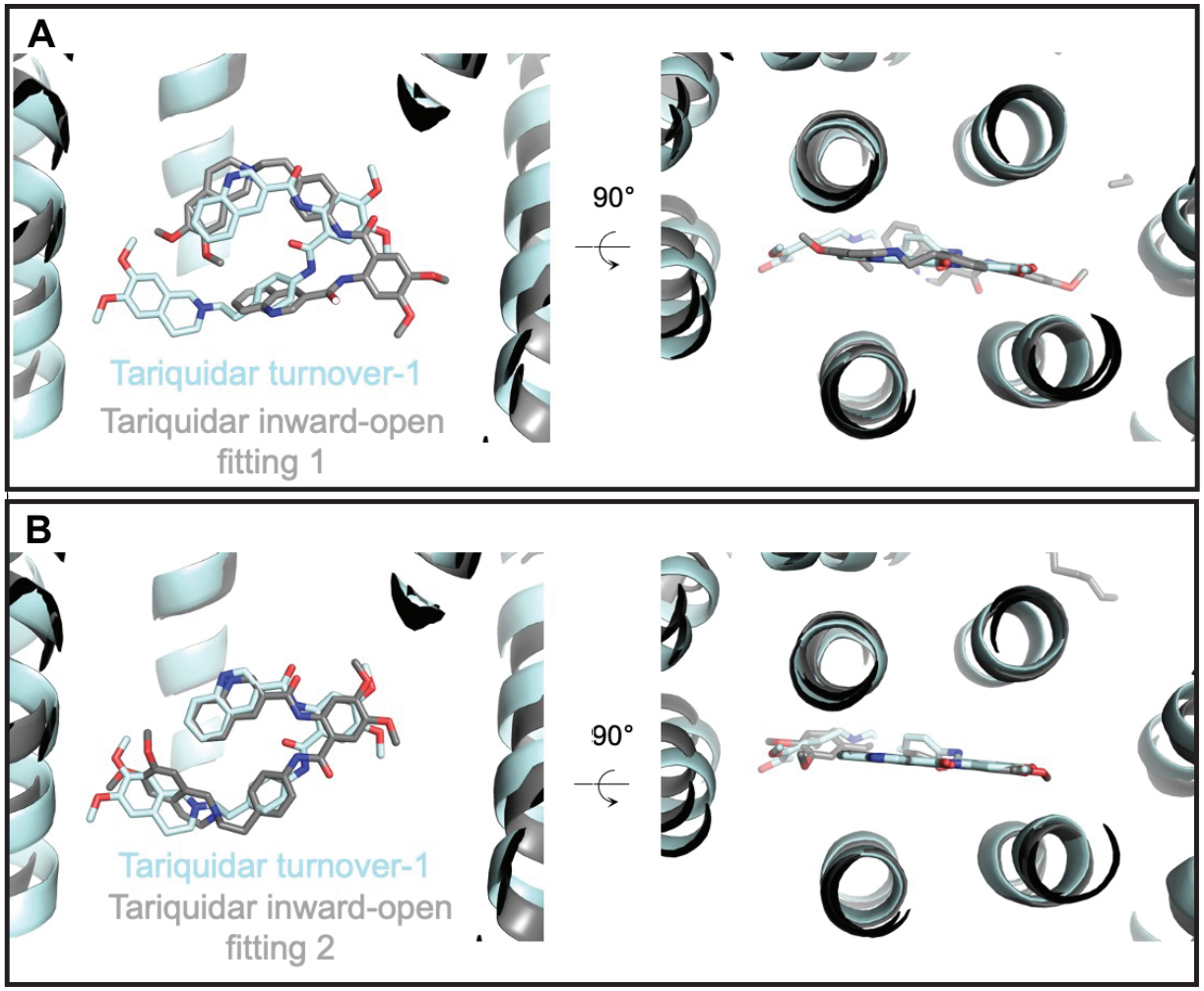

Figure S7: **Comparison of tariquidar in TO1 and IF-open conformations of ABCG2**. **(A)** Left, comparison of tariquidar turnover-1 state and tariquidar inward-open conformation structures fitting 1 (PDB: 7NEQ[17]) are shown in cyan and grey, respectively. To compare the orientation of bound tariquidar in cavity 1, a pair of F439 from each structure, the landmark in the substrate translocation pathway, is used for alignment. Right, rotate 90° along x-axis and showing the top veiew of cavity 1. **(B)** Comparison of tariquidar turnover-1 state and tariquidar inward-open conformation structures fitting 2[17]

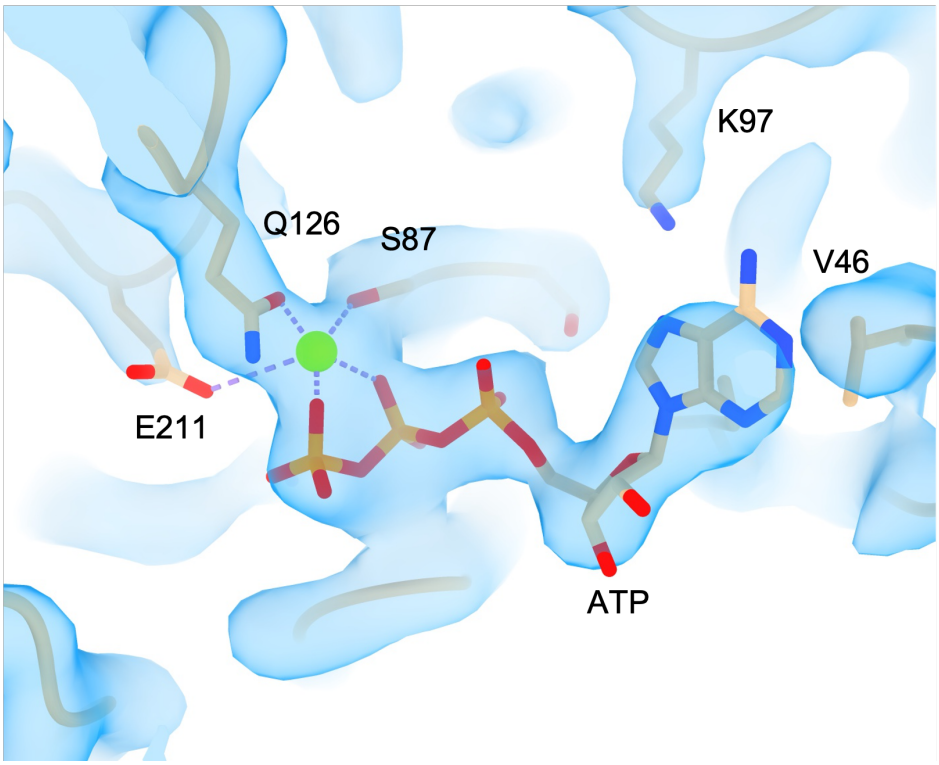

Figure S8: **Closeup view of the nucleotide binding site in the TO2 state**. Non-symmetrized EM density maps are shown as blue surface. The bound nucleotide and key residues are shown as sticks and labeled.

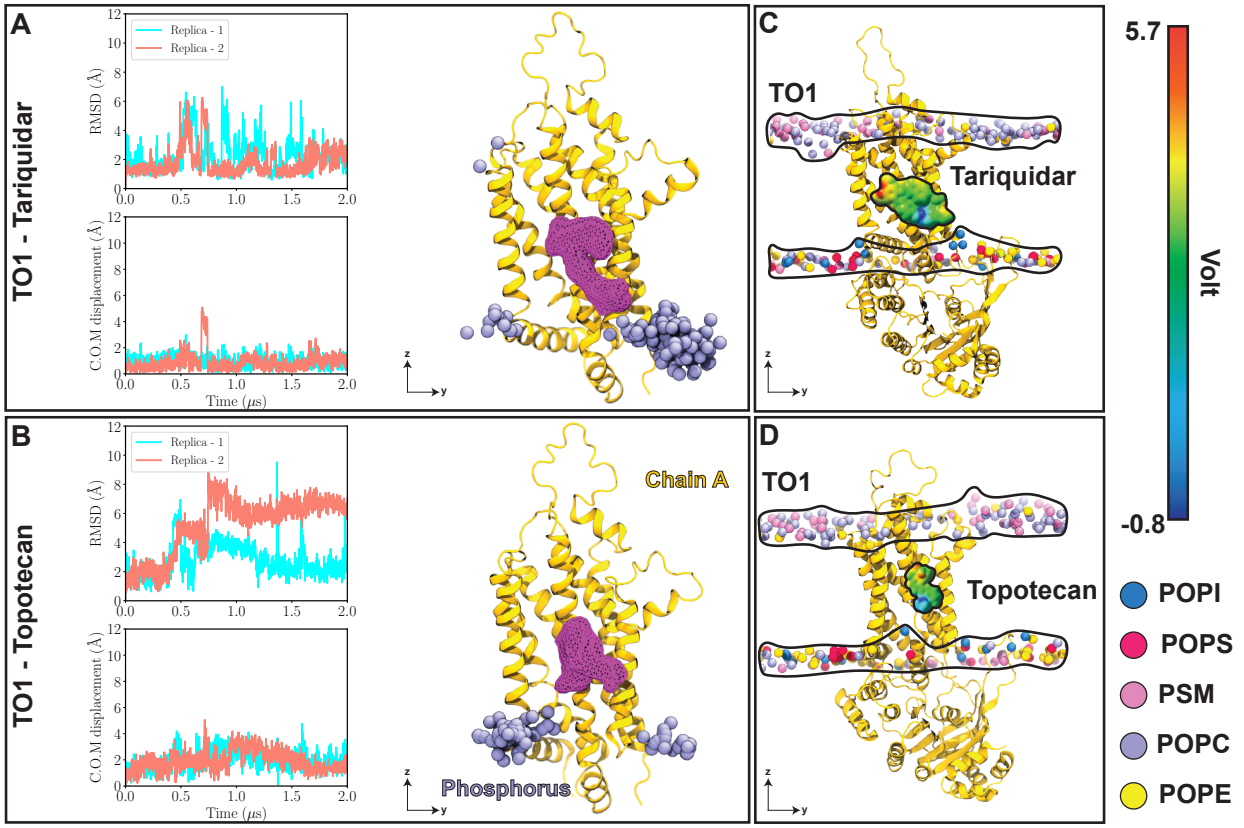

Figure S9: **Ligand fluctuation and protein penetration of lipids for topotecan- and tariquidar-bound TO1 structures. (A)** Left, top: Heavy-atom RMSD of tariquidar with respect to its cryo-EM pose. bottom: Minimal Center of mass distance of tariquidar with respect to its two symmetry-related binding poses in the cryo-EM model. Right, Superimposed snapshots of the phosphorus atoms (purple) that come closer than 20 Å to tariquidar (collected from both TO1 simulated replicas with 125 ns intervals). Spatial density of the ligand obtained from the aggregate of both replicas are shown as a purple mesh at isovalue of 0.3. **(B)** Similar data from topotecan-bound simulations. Topotecan shows much larger fluctuations and is observed to directly interact with lipids. **(C)** and **(D)** Charge-charge interactions between phospholipids and substrates in TO1 state for tariquidar and topotecan, respectively. The electrostatic potential map for each ligand highlights the positive center of each molecule (blue). Topotecan's positive charge is much more accessible for direct interactions/contacts with lipids, whereas tariquidar's positive charge is more buried and less accessible. Phosphorus atoms of different lipids are shown as spheres and colored according to the legend. To provide a clear view into the binding cavity, only Chain A is shown (yellow).

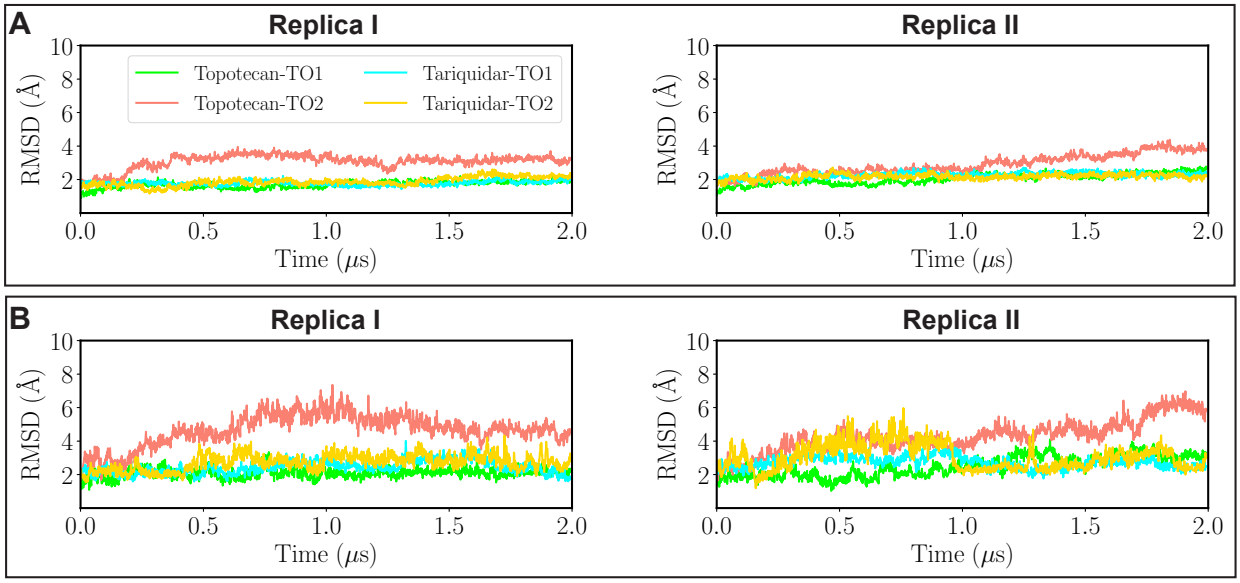

Figure S10: **RMSD of different domains.** C_α RMSD of the TMDs **(A)** and NBDs **(B)** calculated with respect to the initial cryo-EM model during the 2 μs of the production runs.

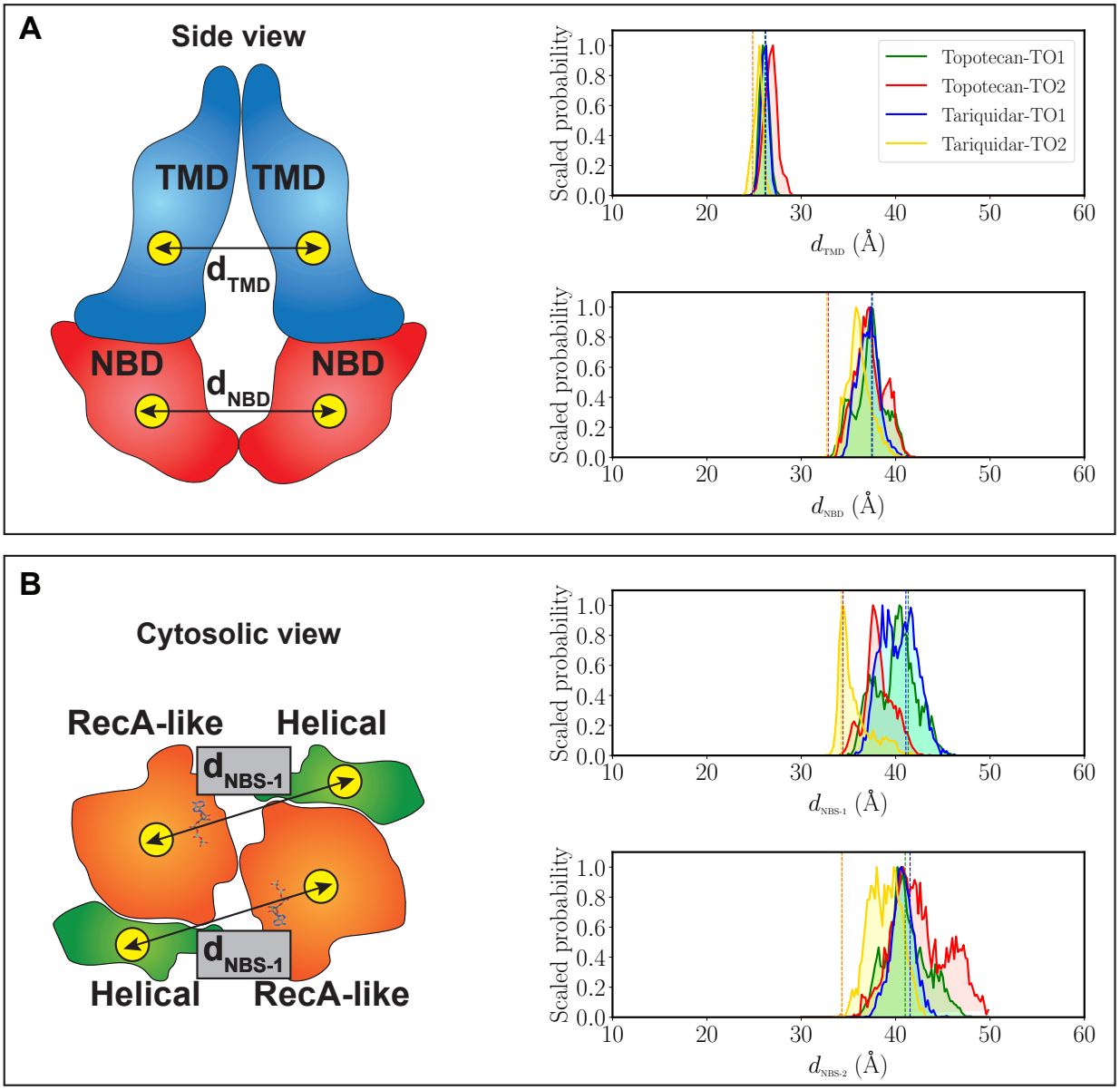

Figure S11: **Domain-domain distances. (A)** Left, schematic representation of the TMD-TMD (d_{TMD}) and NBD-NBD (d_{NBD}) distances, using the center of mass of each domain. Right, distributions of d_{TMD} (top) and d_{NBD} (bottom) accumulated for both replicas during 2 μs of production runs. The distances of the cryo-EM models are represented by dashed lines with the same color as the simulation histograms. **(B)** Left, schematic representation of the RecA-Helical (d_{NBS}) defined for both nucleotide binding sites. Right, distributions of d_{NBS-1} (top) and d_{NBS-2} (bottom) accumulated for both replicas during 2 μs of production runs.

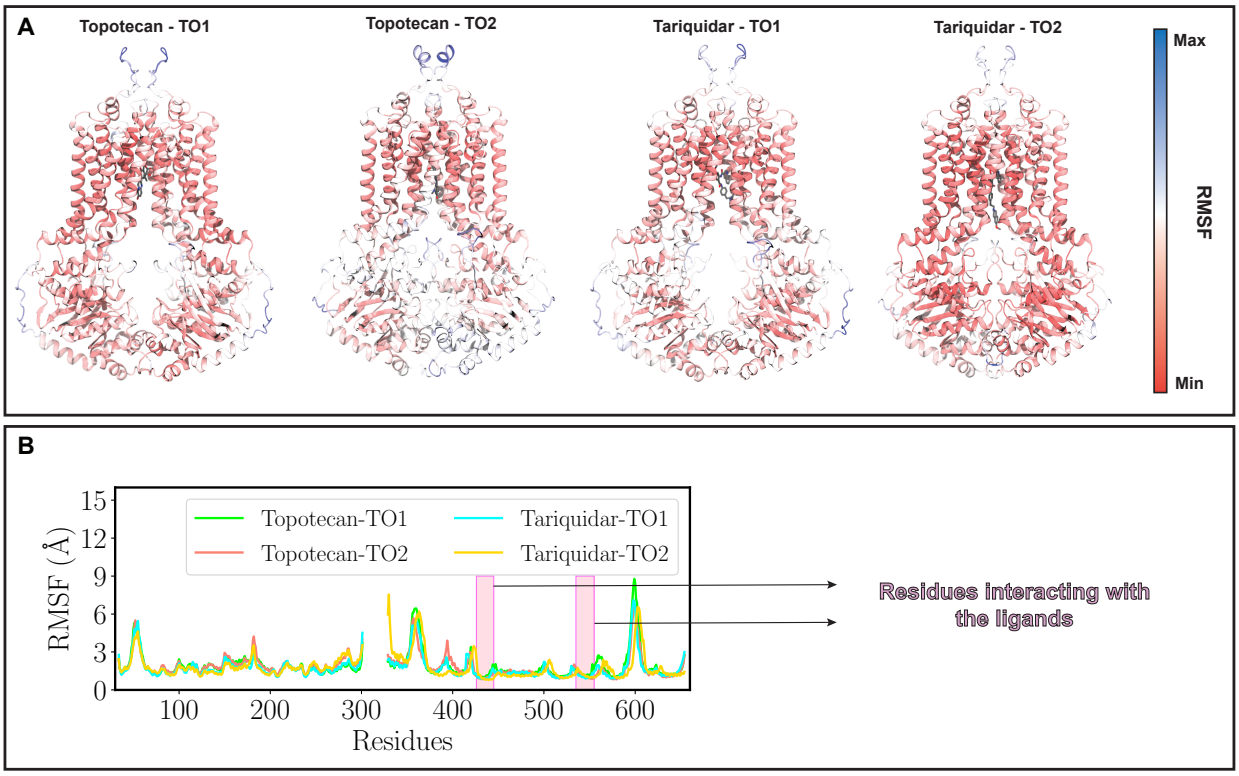

Figure S12: **RMSF of individual residues. (A)** Structures of topotecan- and tariquidar-bound TO1 and TO2 colored based on RMSF of individual residues. **(B)** RMSF of each residue averaged over both replicas. Residues forming the binding pocket (residues: 425-445 and 535-555) are highlighted with pink boxes.

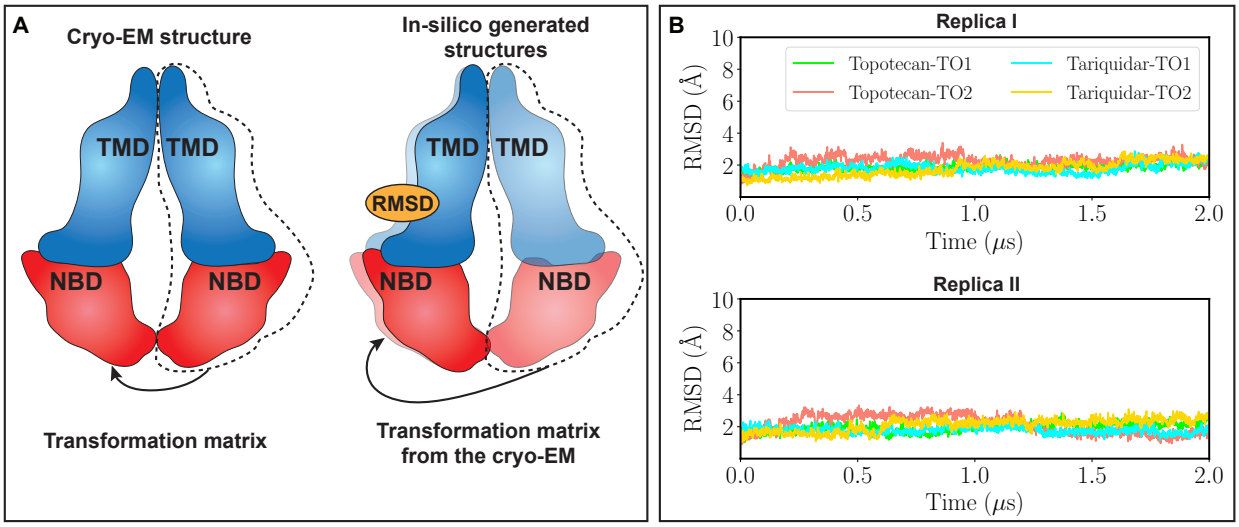

Figure S13: **Symmetry of the TMDs. (A)** The transformation matrix to align the TMDs is calculated from the cryo-EM structure and used in the fit the TMDs during the simulations. The RMSDs are calculated between the transformed protomer (shown in transparent) and the reference protomer. **(B)** RMSD values representing the two-fold symmetry of the protein during the simulation.

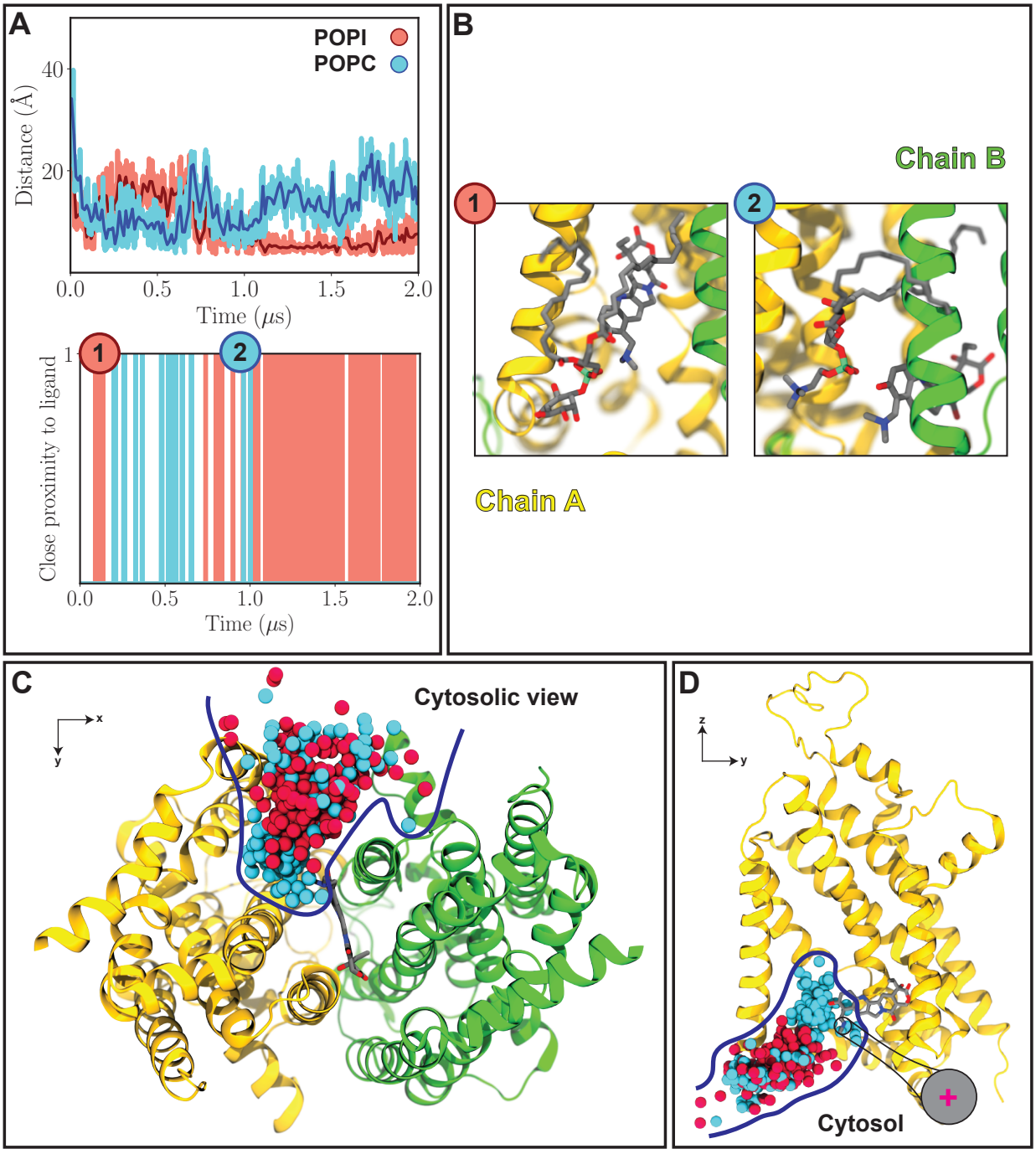

Figure S14: **Lipid penetration into the binding pocket observed in simulation replica 2 of topotecan-bound TO2. (A)** Top: the distance between the phosphorus atom of two lipids that penetrate into the binding pocket (POPI and POPC in red and cyan, respectively) and the titratable nitrogen atom of topotecan. Bottom: instances with lipids and the ligand in close proximity arising during the simulation. **(B)** Representative snapshots of close ligand-lipid contacts. The snapshots correspond to the instances highlighted in **(A)** bottom panel. Chains A and B of the protein are shown in yellow and green, respectively. **(C)** and **(D)** Cytosolic and side views of the trajectory of the lipid phosphorus atoms in the neighborhood of the binding pocket highlighting contacts with topotecan. The phosphorus atoms are colored according to **(A)**. In (C) and (D), the lipid penetration range is outlined with a blue line.

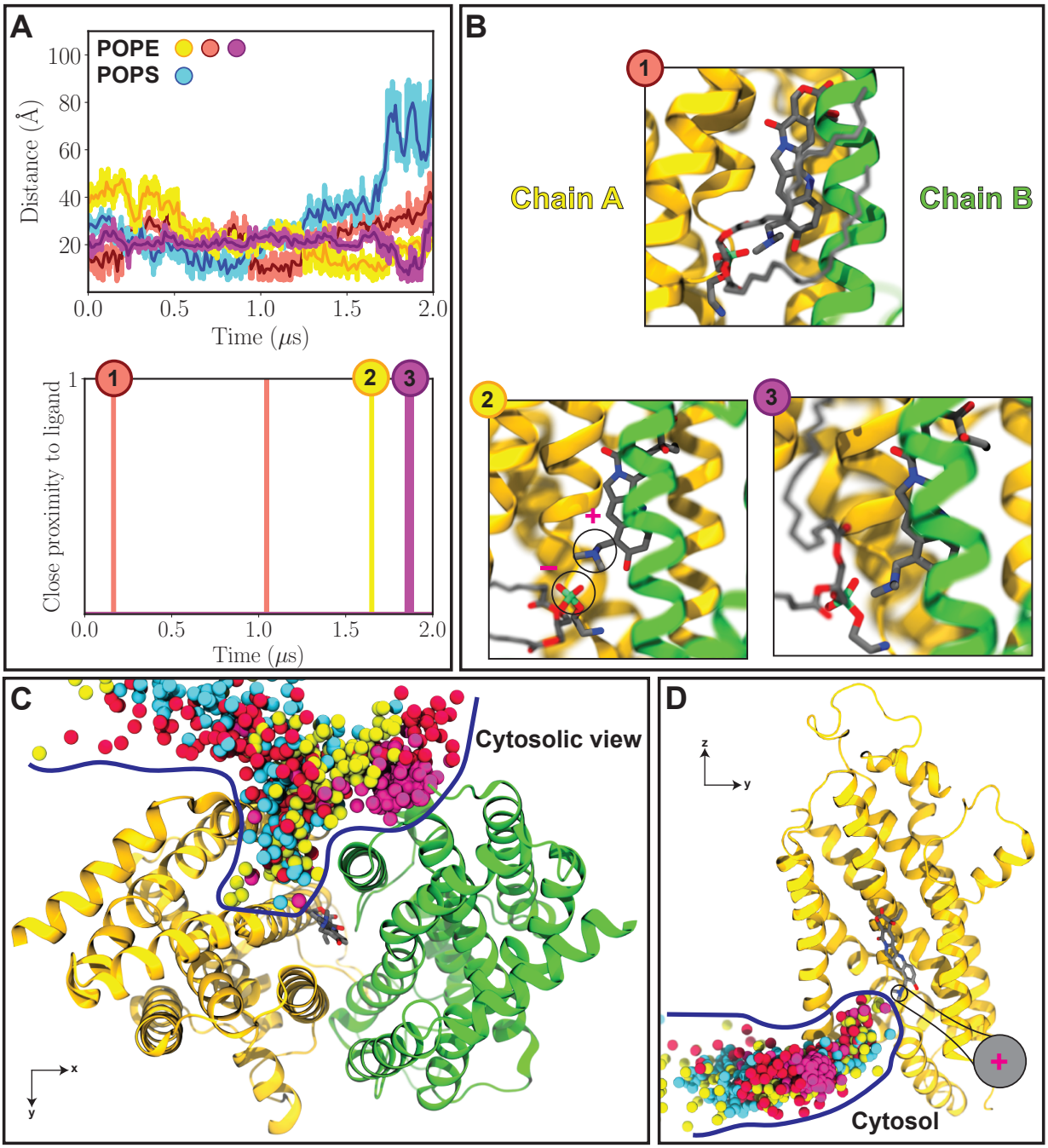

Figure S15: **Lipid penetration into the binding pocket observed in simulation replica 1 of topotecan-bound TO1. (A)** Top: the distance between the phosphorus atom of four lipids that penetrate into the binding pocket (3 POPE and 1 POPS, shown in different colors) and the titratable nitrogen atom of topotecan. Bottom: instances with lipids and the ligand in close proximity arising during the simulation. **(B)** Representative snapshots of close ligand-lipid contacts. The snapshots correspond to the instances highlighted in **(A)** bottom panel. Chains A and B of the protein are shown in yellow and green, respectively. **(C)** and **(D)** Cytosolic and side views of the trajectory of the lipid phosphorus atoms in the neighborhood of the binding pocket highlighting contacts with topotecan. The phosphorus atoms are colored according to **(A)**. In **(C)** and **(D)**, the lipid penetration range is outlined with a blue line.

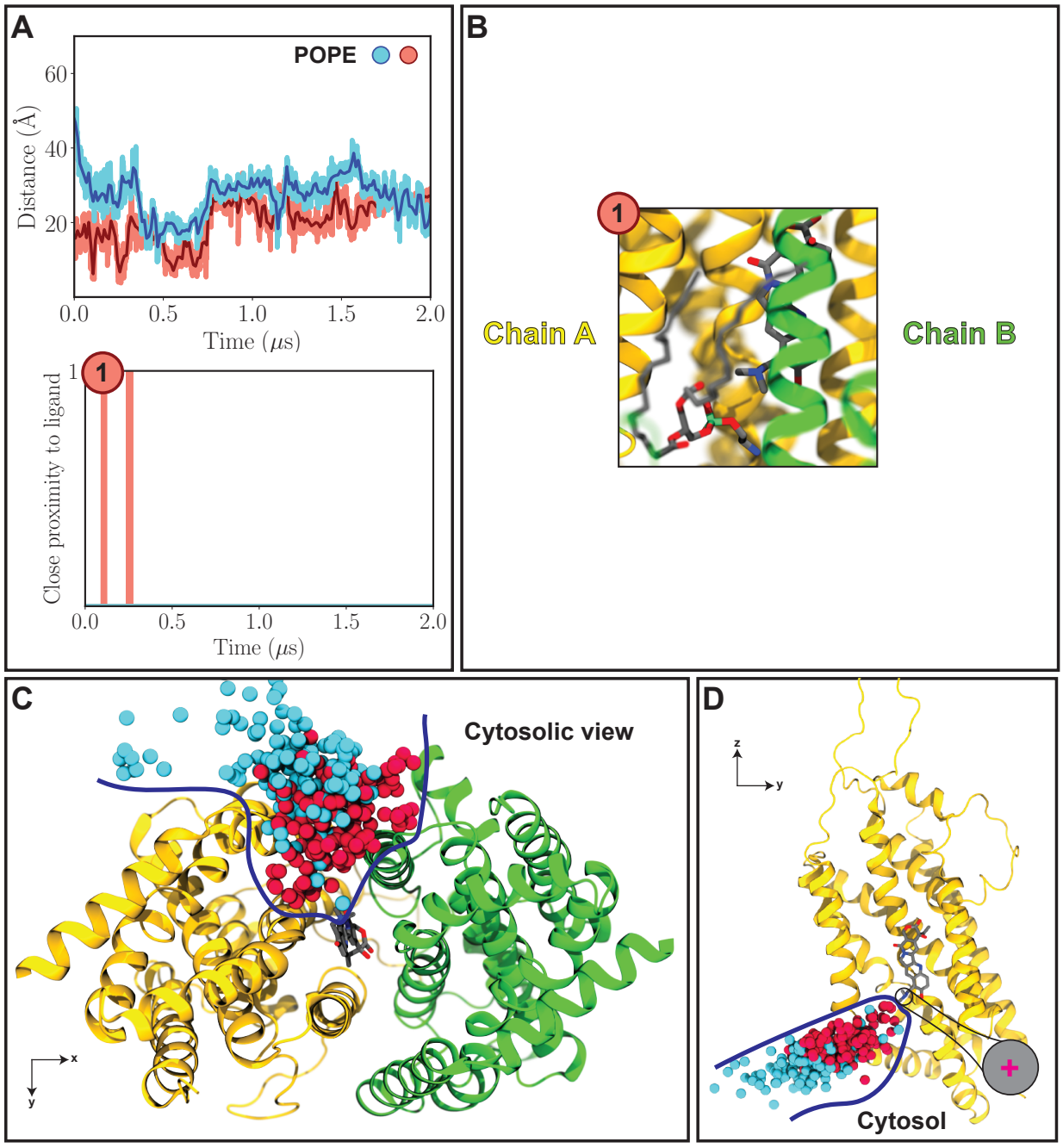

Figure S16: **Lipid penetration into the binding pocket observed in simulation replica 2 of topotecan-bound TO1. (A)** Top: the distance between the phosphorus atom of two POPE lipids that penetrate into the binding pocket (different colors) and the titratable nitrogen atom of topotecan. Bottom: instances with lipids and the ligand in close proximity arising during the simulation. **(B)** Representative snapshot of close ligand-lipid contacts. The snapshot corresponds to the instance highlighted in **(A)** bottom panel. Chains A and B of the protein are shown in yellow and green, respectively. **(C)** and **(D)** Cytosolic and side views of the trajectory of the lipid phosphorus atoms in the neighborhood of the binding pocket highlighting contacts with topotecan. The phosphorus atoms are colored according to **(A)**. In (C) and (D), the lipid penetration range is outlined with a blue line.

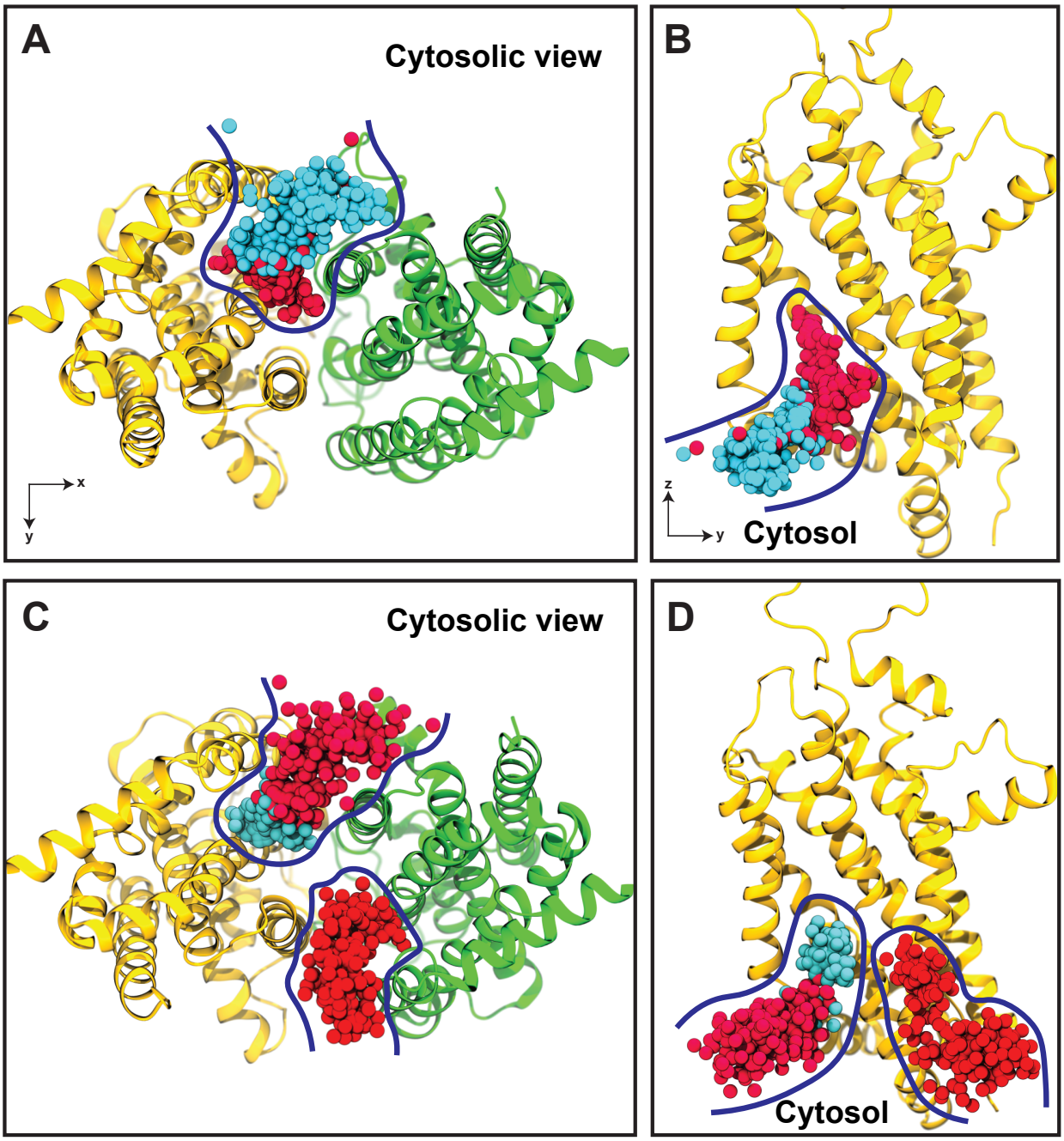

Figure S17: **Lipid penetration into the binding pocket of the IF-apo ABCG2 (A)** and **(B)** Cytosolic and side views of the phosphorus atoms of lipids that penetrate the binding pocket during the 1 μs simulation for simulation replica 1 (red and cyan representing a POPS and a POPE, respectively). Chains A and B of the protein are shown in orange and green, respectively. **(C)** and **(D)** show the data for simulation replica 2 of the same system, this time with red representing two POPS molecules and cyan representing one POPE.

Legends to Supplementary Movies

Supplementary Movie 1. MD trajectory of the tariquidar-bound TO2 state during a 2-μs simulation. ABCG2 is shown in cartoon representation with monomers colored in green and yellow, respectively, and the bound ligands are shown with sticks.

Supplementary Movie 2. MD trajectory of the tariquidar-bound TO1 state during a 2-μs simulation. ABCG2 is shown in cartoon representation with monomers colored in green and yellow, respectively, and the bound ligands are shown with sticks.

Supplementary Movie 3. MD trajectory of the topotecan-bound TO2 state during a 2-μs simulation. ABCG2 is shown in cartoon representation with monomers colored in green and yellow, respectively, and the bound ligands are shown with sticks. Two phospholipids, a POPS (red) and a PSM (cyan), that penetrate the binding pocket are shown.

Supplementary Movie 4. MD trajectory of the topotecan-bound TO1 state during a 2-μs simulation. ABCG2 is shown in cartoon representation with monomers colored in green and yellow, respectively, and the bound ligands are shown with sticks. Two POPE lipids that penetrate the binding pocket during the simulation are shown in red and cyan, respectively.

Supplementary Movie 5. MD trajectory of ABCG2 in IF-Apo conformation during a 1-μs simulation. ABCG2 is shown in cartoon representation with monomers colored in green and yellow, respectively. Two phospholipids that penetrate the binding pocket during the simulation, a POPS (red) and POPE (cyan), are shown.